Structural Studies of Apo NosL, an Accessory Protein of the Nitrous Oxide Reductase System: Insights from Structural Homology with MerB, a Mercury Resistance Protein[†,‡]

Lara M. Taubner,[§] Michele A. McGuirl,[||] David M. Dooley,*[,§] and Valérie Copié*[,§]

Department of Chemistry and Biochemistry, Montana State University, Bozeman, Montana 59717, and Division of Biological Sciences, University of Montana, Missoula, Montana 59812

Received May 31, 2006; Revised Manuscript Received August 11, 2006

ABSTRACT: The formation of the unique catalytic tetranuclear copper cluster (Cu_Z) of nitrous oxide reductase, N_2OR, requires the coexpression of a multiprotein assembly apparatus encoded by the *nosDFYL* operon. NosL, one of the proteins encoded by this transcript, is a 20 kDa lipoprotein of the periplasm that has been shown to bind copper(I), although its function has yet to be detemined. Cu(I) EXAFS data collected on the holo protein demonstrated that features of the copper binding site are consistent with a role for this protein as a metallochaperone, a class of metal ion transporters involved in metal resistance, homeostasis, and metallocluster biosynthesis. To test this hypothesis and to gain insight into other potential functional roles for this protein in the N_2OR system, the three-dimensional solution structure of apo NosL has been solved by solution NMR methods. The structure of apo NosL consists of two relatively independent homologous domains that adopt an unusual $\beta\beta\alpha\beta$ topology. The fold of apo NosL displays structural homology to only one other protein, MerB, an organomercury lyase involved in bacterial mercury resistance (Di Lello et al. (2004) *Biochemistry 43*, 8322−32). The structural similarity between apo NosL and MerB, together with the absolute conservation of Met109 in all NosL sequences, indicates that this residue may be involved in copper ligation, and that the metal binding site is likely to be solvent-accessible and contiguous with a large binding cleft. The structural observations suggest that NosL is exceptionally adapted for a role in copper and/or sulfur delivery and possibly for metallochaperone function.

Nitrous oxide reductase (N_2OR[1]) performs the last step of denitrification, the conversion of nitrous oxide to dinitrogen (N_2), returning nitrogen derived from biomass back to the atmosphere. To accomplish this energetically demanding reaction, N_2OR utilizes two functionally critical multinuclear copper clusters, an electron donor site, Cu_A, and a catalytic site, Cu_Z (*1*). The Cu_A site of N_2OR is a [$Cu_2S(Cys)_2$] copper cluster, essentially identical to the Cu_A site of cytochrome *c* oxidase, and is responsible for the transfer of two electrons from an electron donor to the active site of Cu_Z for N_2O reduction (*2*). Cu_Z is a novel metal center consisting of four copper atoms arranged in a distorted tetrahedron with an inorganic sulfide bridging the metal ions at the apex (*3*). Formation of this complex catalytic cluster requires copper and sulfur, both of which have been shown to utilize specifically dedicated uptake and transport systems in order to prevent undesirable side reactions and to ensure delivery to the appropriate physiologic targets. Thus N_2OR is a member of a now widely recognized class of complex metalloenzymes that require a variety of accessory, transport, and cofactor insertion proteins for assembly of essential metalloclusters.

The *nosDFY* operon, located downstream of the N_2OR structural gene, *nosZ*, has been implicated in Cu_Z biogenesis. Based on sequence analysis of the translated genes, the three proteins encoded by *nosDFY* are predicted to bear topological and functional similarity to the ABC or ATP-binding cassette transporter superfamily, which are multicomponent assemblies that are used ubiquitously by archaeal, eubacterial, and eukaryotic organisms for small molecule transport across membranes (*4*). In the *nos* system, these components are believed to provide the machinery designed to couple ATP/GTP hydrolysis to copper and/or sulfur insertion into the Cu_Z cluster of N_2OR that occurs posttranslocationally within the periplasm (*5*). NosF is a peripheral cytoplasmic protein

[†] This work was supported in part by the National Science Foundation, Grants MCB-0444056 (V.C.) and MCB-0347871 (D.M.D.). The NMR experiments were recorded at Montana State University on a DRX600 spectrometer, purchased in part with funds from the NIH shared instrumentation grant program (SIG Grant 1-S10RR13878-01), and the NSF-EPSCOR program for the State of Montana.

[‡] PDB accession codes: The average energy-minimized structure, as well as an ensemble of 20 lowest energy structures, has been deposited in the protein data bank, ID codes 2HQ3, and 2HPU, respectively.

* Correspondence should be addressed to these authors: Department of Chemistry and Biochemistry, Montana State University, Gaines Hall Room 108, Bozeman, MT 59717. Tel: 406-994-7244. Fax: 406-994-5407. E-mail: vcopie@chemistry.montana.edu.

[§] Montana State University.

[||] University of Montana.

[1] Abbreviations: ABC, ATP binding cassette; DIPSI, decoupling in the presence of scalar interactions; DTT, dithiothreitol; DSS, 2,2-dimethyl-2-silapentane-5-sulfonic acid; EDTA, ethylenediaminetetraacetic acid; EPR, electron paramagnetic resonance; EXAFS, extended X-ray absorption fine structure; HSQC, heteronuclear single quantum coherence spectroscopy; IPTG, isopropyl β-thiogalactoside; MOPS, 3-(*N*-morpholino)propanesulfonic acid; NMR, nuclear magnetic resonance; NOESY, nuclear Overhauser enhancement spectroscopy; N_2-OR, nitrous oxide reductase; NOE, nuclear Overhauser effect.

10.1021/bi061089+ CCC: $33.50
Published on Web 09/19/2006

with confirmed ATPase activity, capable of providing energy for metal or small molecule transfer (*6*). NosY is predicted to be an integral membrane protein containing six transmembrane helices, believed to transduce the energy generated from ATP hydrolysis by NosF. NosD is a 45 kDa hydrophilic periplasmic constituent of unknown function expected to contain a β-helical domain, as evidenced by its sequence homology to the CASH (carbohydrate-binding and sugar hydrolase) superfamily of proteins (*7*). Biosynthesis of the Cu_Z copper center has been shown to require the coexpression of the NosD, NosF, and NosY proteins (*5*).

An additional gene downstream of *nosDFY*, *nosL*, is cotranscribed along with the rest of the gene cluster, indicating a role for this gene product in N_2OR assembly (*5*, *8*). Tn5-mediated mutagenesis interruption of the C-terminus of NosL, however, had no effect on N_2OR synthesis in *Pseudomonas stutzeri* (*8*). Expression of the *nosZDFY* genes from *P. stutzeri* in *Pseudomonas putida*, a nondenitrifying organism, was sufficient for the production of catalytically competent N_2OR, confirming that NosL is not obligatory for Cu_Z or Cu_A biosynthesis or that there is a "rescue" substitute in the host (*5*). Unlike additional *nos* genes that are not conserved, NosL is consistently present in all denitrifying genomes sequenced thus far, including those in which the relative order of the *nosDFYL* genes is not conserved, suggesting an important yet unidentified function for this protein in N_2OR maturation.

The translated sequence of *Achromobacter cycloclastes* (*A. cycloclastes*) NosL (*9*) contains a putative lipobox, (L(A/S)(G/A)C), a signal peptide that targets the protein for translocation through the inner membrane, followed by cleavage of the signal leader sequence and amino-acylation of the N-terminal cysteine to diacylglycerol (*10*). NosL is most likely shuttled through the periplasm where the resulting anchor tethers the protein to the outer membrane. Other than the secretion signal, the sequence of this 20 kDa protein exhibits little similarity to other sequences of proteins of known functions and therefore reveals little about the potential role of this protein in N_2OR assembly. Alignment of NosL sequences from *A. cycloclastes* (*9*, *11*), *Bradyrhizobium japonicum* (*12*), *Pseudomonas aeruginosa (13*), *Paracoccus denitrificans* (*14*), *P. stuzeri* (*15*), *Sinorhizobium meliloti* (*16*), and *Rhodobacter sphaeroides* (*17*), i.e., well-studied denitrifying organisms with well-characterized N_2OR sequences, reveals that, of the few conserved residues within this relatively divergent group, there are only two readily identifiable motifs of unknown function(s), CXMXXX-(E/D)XPGPK(G/A)(E/Q) and G(G/A)XMGA (*9*) (see alignment in Supplementary Figure S1 (Supporting Information)). Inclusion of additional NosL sequences in the NCBI databank reduces the conserved motifs to PGPK and (G/A)XMG. Interestingly, within these sequences, no readily discernible copper-binding motif is present (*18*).

Experiments conducted on the recombinant protein from the facultative anaerobe *A. cycloclastes*, which lacks the lipid anchor and has a Met-Asp insertion at the N-terminus of the mature protein, demonstrated that NosL contains one Cu(I) atom per monomer (*18*). Exposure to aerobic conditions resulted in the loss of copper and dimerization via intermolecular disulfide bond formation. Extended X-ray absorption fine structure (EXAFS) spectroscopy indicated that the Cu(I) coordination is best described as being three-coordinate, with one nitrogen/oxygen donor and two sulfur ligands. The lack of reactivity of the sole Cys residue of the recombinant protein with reagents that detect free thiols suggested that this cysteine is unavailable due to Cu(I) coordination (*18*). The relatively recent discovery of a methionine-rich high-affinity Cu(I) binding motif, MX_nM, specific for periplasmic metal uptake, suggests that the sulfur ligands in NosL could be derived from Met residues (*19*−*21*). In the alignment described above, NosL contains two positionally conserved methionine residues, Met26 and Met109, which could serve as copper ligands (see Supplementary Figure S1).

The unique nature of the NosL copper center, which binds Cu(I) and releases it upon oxidation, suggests that it may be involved in copper transport to or assembly of the catalytic Cu_Z or the electron-transfer Cu_A multinuclear copper clusters of N_2OR (*18*). If so, NosL would be a member of the rapidly expanding class of proteins known as metallochaperones: these are proteins involved in metal resistance, homeostasis, or metallocluster assembly, and they serve to protect the cell from the effects of toxic metal ions and ensure delivery to the appropriate metalloenzyme targets (*22*).

We have determined the three-dimensional solution structure of the apo form of NosL (referred to as apo NosL) lacking the lipid moiety by multidimensional solution NMR in order to gain insight into the potential role of this protein in N_2OR metallocluster assembly. To date, this is the first detailed structure of an accessory protein from the *nos* cluster of the N_2OR system. The apo NosL structure consists of a well-defined protein core, held in place by the interactions of two structurally homologous domains that adopt a unique $\beta\beta\alpha\beta$ topology, and two lengthy disordered termini. Features of the fold and the identification of the close structural homologue MerB implicate one of the conserved methionine residues, Met109, in metal binding and provide the structural basis for a copper (and/or sulfur) delivery function in the N_2OR system.

EXPERIMENTAL PROCEDURES

Expression and Purification. Recombinant *A. cycloclastes* NosL was cloned and expressed in *E. coli* using strain BL21-(DE3)/pL46 as reported in ref *18*. The pL46 construct is based on the pET20b(+) vector (Novagen Inc.) and encodes a PelB leader sequence that permits secretion of the protein into the periplasm. Residues encoding the native secretion signal sequence and the N-terminal Cys of the mature protein thought to be lipidated in vivo were omitted to aid in purification. As a result of the cloning protocol, the recombinant apo NosL protein contains a non-native Met-Asp sequence at the N-terminus and lacks the leader sequence (the first 20 N-terminal residues of the full sequence reported in the protein databank, accession number CAA75429). Numbering of the recombinant apo NosL protein used in the NMR studies thus begins at Met1-Asp2-Lys3-Glu4-, where Lys3-Glu4 of apo NosL corresponds to Lys21-Glu22 of the full NosL sequence reported in the PDB (*18*). ^{15}N and ^{13}C uniformly labeled recombinant apo NosL was produced by growing *E. coli* cell cultures in MOPS media enriched with $[^{15}N]NH_4Cl$ (99% ^{15}N-enriched, CIL, Cambridge, MA) or $[^{15}N]NH_4Cl$/D-glucose-$^{13}C_6$ (99% ^{13}C-enriched, CIL, Cambridge, MA) as the sole nitrogen and

carbon sources, respectively. Cultures were grown to an $OD_{600\,nm}$ of approximately 0.7 at 37 °C, followed by induction of protein synthesis with 1 mM IPTG, and subsequent growth at 20 °C for 10 h. Cells were harvested, and the periplasmic apo NosL protein was extracted via osmotic shock. The protein was purified as previously described using DEAE-FF (Sigma Co., St. Louis, MO) ion exchange chromatography, followed by a final purification step using a Resource Q (Amersham Pharmacia Inc., Piscataway, NJ) chromatographic column (*18*). Apo NosL-containing fractions were dialyzed against NMR buffer (100 mM sodium phosphate, 1 mM DTT, 1 mM EDTA, pH 6.5) and concentrated using an Amicon stirred cell (Millipore Inc., Bedford, MA) under argon using a 10 kDa cutoff ultrafiltration membrane. Final NMR samples consisted of 1.0 to 1.5 mM protein in 100 mM sodium phosphate, 1 mM DTT, 1 mM EDTA in either 90% H_2O/10% D_2O or 100% D_2O at a pH of 6.5. Asymmetric flow field flow fractionation/dynamic light scattering experiments were conducted on an AF2000 Focus instrument (PostNova, Inc).

NMR Spectroscopy. All NMR spectra were acquired at 30 °C on a four-channel Bruker DRX-600 spectrometer, with a triple ^{15}N, ^{13}C, ^{1}H inverse resonance probe equipped with triple axis gradients. Quadrature detection for all multidimensional NMR experiments was achieved using the States-TPPI method (*23*). Data were processed and analyzed using the NMRPipe (*24*), PIPP (*25*), NMRView 5.0 (*26*), and XWINNMR version 3.1 (Bruker Inc., Billerica, MA) software packages. Two-dimensional $^{1}H-^{15}N$ HSQC spectra (*27*) were acquired with a spectral width of 14.0 ppm in t_2 and 40.0 ppm in t_1, with the proton carrier frequency set at 4.7 ppm and the nitrogen carrier set at 116.0 ppm. Data were collected with 1024 complex points in t_2 and 128 complex points in t_1, using Waltz-16 (*28*) for ^{15}N decoupling during data acquisition. Apodization was performed using a sine bell squared function shifted by 0.35 π radians in t_2, and a sine bell function shifted by 0.40 π radians in t_1.

Sequential and intraresidue ^{1}H, ^{15}N, and ^{13}C backbone and side-chain chemical shift assignments were extracted from a series of double and triple resonance NMR experiments (HNCA (*29*), HNCO (*29*), HNCACB (*30*), CBCA(CO)NH (*31*), C(CO)NH (*32*), HCC(CO)NH (*32*), $^{1}H-^{13}C$-CT HSQC (*33*) and HCCH-TOCSY (*34*)). $^{1}H-^{13}C$-CT HSQC and HCCH-TOCSY experiments were performed in D_2O. A DIPSI pulse sequence scheme (*35*) was utilized for ^{1}H decoupling during carbon evolution and the Waltz-16 scheme (*28*) for ^{15}N decoupling during data acquisition. Similar apodization functions were used in all spectral dimensions, using shifted sine bell functions.^{1}H, ^{13}C, and ^{15}N, chemical shifts were indirectly referenced to DSS, using absolute frequency ratios for ^{13}C and ^{15}N chemical shift referencing. A detailed description of all acquisition parameters for these experiments and the NOESY experiments described below are included in Supplementary Table 1 (Supporting Information).

Protein Structure Calculations. NOE data collected to derive $^{1}H-^{1}H$ distance restraints for secondary and three-dimensional structure determination were obtained from 3D ^{15}N NOESY experiments (*36*, *37*) with mixing times (t_{mix}) of 100, 120, and 140 ms and from 3D HCHC-NOESY (*38*) (t_{mix} = 140 ms) spectra acquired at 600 MHz. Additional ^{15}N NOESY-HSQC and ^{13}C NOESY-HSQC experiments (NOE mixing times of 120 ms) were acquired on a Varian 800 INOVA (800 MHz) instrument at the Environmental Molecular Sciences Laboratory (EMSL), sponsored by the Department of Energy's Office of the Biological and Environmental Research, located at the Pacific Northwest National Laboratory (PNNL).

^{13}C- and ^{15}N-edited NOESY spectra were processed using NMRPipe and imported into NMRView 5.0. NOE cross peaks were annotated in NMRView using the standard peak-picking algorithm and the associated volumes collected. Cross peaks corresponding to intraresidue and sequential NOEs, and NOEs arising from secondary structure spin network, were assigned manually. A total of 112 NOEs were assigned in this fashion and entered into an NOE cross peak list. At this stage, unassigned peaks annotated by NMRView but believed to be artifacts were deleted from the list. The resulting NOE cross peak files and chemical shift information, along with the primary sequence of apo NosL, were used as input into the program ARIA 1.2 (Ambiguous Restraints for Iterative Assignment) (*39*−*41*).

The ARIA calculation proceeded in nine iterations of NOESY spectra calibration and assignment of ambiguous and unambiguous distance restraints followed by calculation of an ensemble of structures. By default, ARIA calibrates distance restraints by computing the relaxation matrix from the NOE peak intensities and the chemical shift assignments (*40*). A rotational correlation time of 9 ns was used for computation of the relaxation matrix. More precise structures (with lower mean rmsds) were obtained using the standard r^{-6} dependence of the NOE volumes and the isolated spin pair approximation implemented in ARIA to calibrate the distance restraints (*39*). Within the NOE assignment protocol, unassigned NOE cross peaks were matched to each possible chemical shift within a frequency tolerance range of ±0.04 ppm for protons and ±0.4 ppm for nitrogen or carbon heteronuclei, generating several potential NOE assignments. These assignments were then treated by the ARIA program as ambiguous distance restraints (*39*, *41*).

The total number of ambiguous NOE restraints allowed for each peak in the NOESY data was set to 7 (max_n). Iteration zero was used to generate the initial ensemble of structures and set to an NOE violation tolerance (vtol) of 1000 Å to ensure that no NOE distance restraints were excluded, and with a partial assignment cutoff probability (also called ambiguity cutoff) (ρ) set to 1.01 to ensure that partial NOE assignments were based on chemical shifts only during this first iteration cycle (*39*). For subsequent iterations, the violation tolerances were set to vtol = (1000, 1.0, 0.5, 0.1, 1.0, 0.1, 0.1, 0.1) and the ambiguity cutoffs (ρ) set to ρ = (0.9999, 0.999, 0.98, 0.96, 0.93, 0.90, and 0.80). For iterations one through eight, the average distance information from the 20 lowest energy structures from an ensemble of 100 was used as the basis for NOE assignment and calibration in the next cycle. For each ARIA run, a total of nine iterations were performed followed by refinement in explicit solvent (*42*), using the ARIA parameters described above and similar to the default values reported in ref *40*.

For the structure calculation step in each cycle, ARIA invoked the software suite Crystallography and NMR System 1.0 (*CNS*) (*43*), using the automatically and manually assigned NOE-derived distance information, hydrogen bond distance restraints, and dihedral angle data, as input restraints

for the calculation, starting from an extended structure. Hydrogen bond restraints were obtained by monitoring the disappearance of amide proton resonances upon exchange with deuterium in a series of 2D $^{1}H-^{15}N$-HSQC spectra. To perform the H/D exchange experiments, a highly concentrated sample of apo NosL was rapidly diluted with D_2O-containing buffer and reconcentrated quickly, followed by NMR data acquisition. The shortest time point between the start of the H/D solvent exchange process and completion of the first HSQC spectrum was approximately 30 min. Inferred nitrogen−oxygen distances were given the lower distance bound of 2.5 Å and an upper distance bound of 3.3 Å. Hydrogen bond distance restraints between the amide proton and oxygen were given a lower bound of 1.5 Å and an upper bound of 2.3 Å. The program TALOS (*44*) generated ϕ and ψ dihedral angle restraints based on observed chemical shifts for Ca, Cb, CO, N, and Hα except for those shifts that yielded ambiguous dihedral angle values. To facilitate convergence, residues Met1−Pro34 and residues Glu161−Gly175 were omitted from the structural calculations based on the observation that these residues either lacked useful chemical shift information or demonstrated little if any NOE signals, an indication that these regions of apo NosL, corresponding to the N- and C-termini of the protein, are disordered and in all likelihood floppy.

Following each computational cycle of ARIA, resulting structures were manually inspected and remaining restraint violations analyzed. During this step, large violations were removed (those yielding energies of roughly >100 kcal/mol), and the ARIA calculations were repeated using NMR assignments generated from previous ARIA iterations until convergence was achieved. For the final set of ARIA calculations, 100 structures were generated and 20 lowest energy structures selected for analysis using the programs Quanta (Molecular Simulations Inc.), MOLMOL (*45*), PROCHECK-NMR (*46*), and GRASP (*47*). A total number of 1677 NOEs (780 intraresidue restraints and 897 interresidue restraints), 146 dihedral angle restraints, and 76 hydrogen bond restraints were used as experimental restraints and input into ARIA/CNS. Structural homologues were identified by submitting three of the lowest energy structures to the DALI (*48*, *49*) server (www.ebi.ac.uk/dali) as a web request. The average energy-minimized structure, as well as an ensemble of 20 lowest energy structures, has been deposited in the protein data bank, ID codes 2HQ3 and 2HPU, respectively.

RESULTS

NMR Chemical Shift Assignments and Determination of the Secondary Structural Elements of Apo NosL. Excluding apo NosL's 14 proline residues, 11 out of a total of 161 amide resonances remained unassigned following chemical shift identification, corresponding to a sequential assignment of 93%. Amide resonances for Met1, Asp2, Thr16, Leu20, Tyr23−Leu28, and Ser50 of apo NosL could not be readily discerned and are presumed to be involved in conformational exchange processes that broaden signals beyond detection in the HSQC spectrum. 166 of Cα and 141 of CO chemical shifts out of a possible total of 175 were obtained, and 94% of Hα and Hβ assignments were achieved. Backbone and side chain (^{1}H, ^{15}N, ^{13}C) resonance assignments have been deposited in the BioMagResBank database under the accession number 5595 (*50*). In some of the ^{15}N and ^{13}C spectra, a few of the resonances appeared doubled (Asn74 and Ala55), suggesting that these residues may be undergoing motional dynamics in the slow exchange regime. To verify that apo NosL is monomeric under the conditions used for NMR, asymmetric flow field low fractionation/dynamic light scattering experiments were conducted and demonstrated that, consistent with the spectral line widths observed in the NMR, apo NosL is not engaging in significant monomer−dimer equilibria (McGuirl et al., unpublished).

Cα, Cβ chemical shifts, NOEs, and protection from hydrogen/deuterium exchange data were used to identify the secondary structural elements of apo NosL and to determine β strand topology (Figure 1). The protein secondary structure consists of seven β strands, two α-helices, and two 3_{10} helices punctuated by loops of varying lengths. The β strands are arranged into two antiparallel β sheets, denoted as sheet A and sheet B. A schematic diagram displaying the hydrogen bonding pattern and NOE connectivities in the two sheets is shown in Figure 2. The N- and C-termini of apo NosL, extending from residues Met1−Pro34 and Val145−Gly175 respectively, yielded very few characteristic NOEs or hydrogen bonds, and no significant chemical shift deviations from random coil values (*51*), consistent with lack of structure for these regions (Figure 1).

β sheet A is composed of four strands extending from residues Ala36−Leu40 (β1), Leu47−Phe49 (β2), Val70−Asn74 (β3), and Asn90−Ala93 (β4) (Figures 1 and 2). Strand β3 of sheet A contains a β-bulge centered at Leu40, the carbonyl oxygen of which interacts with the amide proton of residues Ile68 and Leu69. The other β sheet, sheet B, is composed of three strands consisting of residues Phe98−Gly102 (β5), Glu113−Phe117 (β6), and finally Gly132−Ala136 (β7) (Figures 1 and 2). The first α-helix (a1) encompasses residues Val52−Ala59 following strand β2 after a short linker region. The second α-helix (α2), positioned between strands β6 and β7, consists of residues Arg120−Ala129. Residues Leu137−Ile140 and residues Ala94−Ala97 each form a 3_{10} helix, as identified by the characteristic $d_{\alpha N}$ (i, $i + 2$) NOEs and hydrogen bonding pattern (Figure 1).

Three-Dimensional Structure of Apo NosL. Once the secondary structure elements of apo NosL were established, the global fold of the protein was identified using the structural calculation software package ARIA 1.2 (41). A total of 112 manual assignments corresponding primarily to secondary structure, sequential, and intraresidue NOEs were entered into the ARIA program in order to facilitate the automated assignment process.

Initial calculations of full-length apo NosL (spanning residues Met1 through Gly175) structures did not converge sufficiently, most probably because of the chemical shift degeneracy for residues in the N- and C-termini, which produced consistently high energy NOE violations after final water refinement. To circumvent this problem, residues starting from Lys35 to Glu160 in the apo NosL sequence were used as a starting template in order to simplify possible chemical shifts and potential NOE assignments made by ARIA, and to facilitate convergence. As mentioned, residues in the protein segments omitted from the calculations displayed very few nonsequential NOE signals, suggesting these N- and C-terminal regions of the protein have little

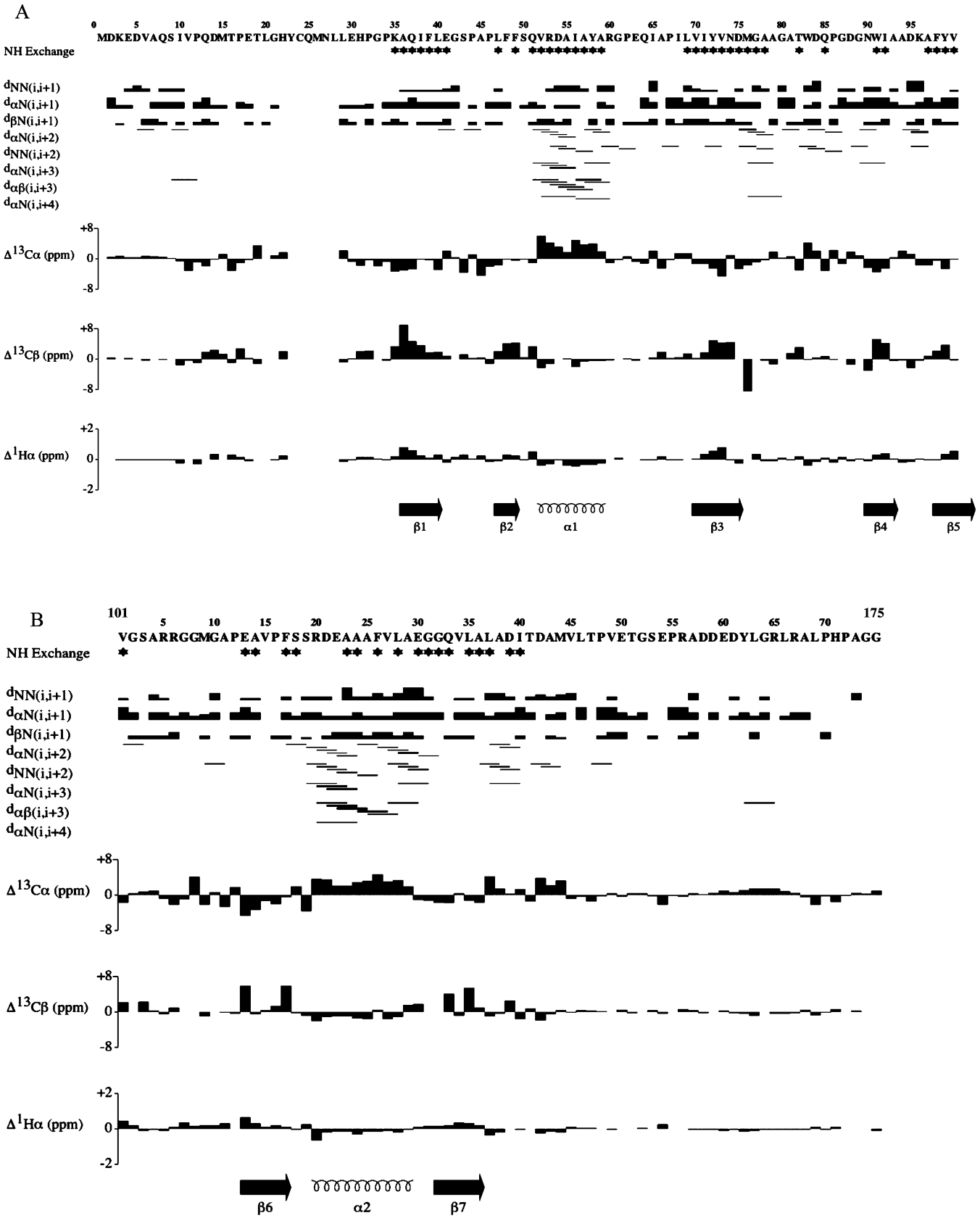

FIGURE 1: Summary of amide H/D exchange data, patterns of sequential and short-range NOEs, and secondary chemical shifts for residues 1−100 (A) and 101−175 (B) of apo NosL. The height of the box for the NOE data reflects the intensity of each NOE cross peak detected in ^{15}N- and ^{13}C-edited ^{1}H−^{1}H NOESY spectra. Differences in ppm for ^{13}Cα, ^{13}Cβ, and ^{1}Hα chemical shifts relative to random coil values are shown. The last row delineates the consensus secondary structure elements identified from the NMR parameters depicted above.

well-ordered structural features. The disorder of the N- and C-termini of apo NosL may also explain why previous attempts at crystallizing the protein had failed. Regrettably, one of the two conserved motifs identified by alignment of NosL sequences, CXMXXX(E/D)XPGPK(G/A)(E/Q), is part of the region of the recombinant protein lacking useful NMR

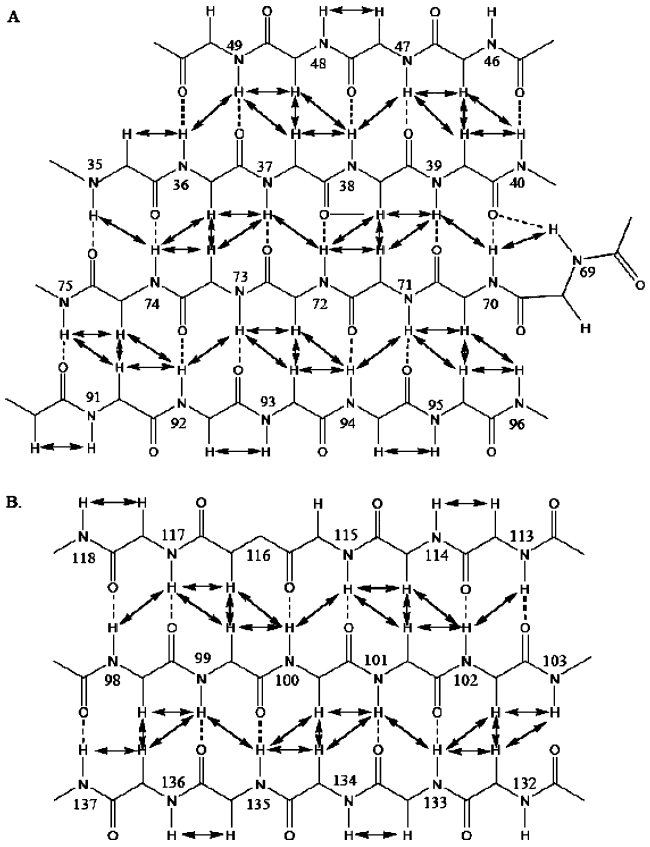

FIGURE 2: Hydrogen bonding network and NOE connectivities detected across β strands for apo NosL as inferred from the NMR data. (A) The β strand topology for the first four-stranded antiparallel β sheet of apo NosL. (B) The H-bond network and NOEs identified in the second, three-stranded antiparallel β sheet of the protein. Hydrogen bonds are indicated by dotted lines, and NOE interactions by double arrows.

information, and therefore could not be meaningfully modeled in the NMR ensemble of apo NosL structures.

Structural determination of apo NosL was initiated starting with calculations of a set of 100 structures using CNS (*43*). From the initial set of 100, 20 lowest energy structures were selected for final analysis, overlaid and displayed in Figure 3. Backbone root-mean-square deviations (rmsd) for the final set of 20 apo NosL structures relative to the mean structure were 0.52 Å for residues located in the well-defined secondary structural elements of the protein, and 1.33 Å for all backbone atoms (Table 1). Dihedral angle mapping on Ramachandran plots using PROCHECK-NMR demonstrated that less than 1% of residues fall within disallowed regions of ϕ/ψ angle space (shown in Supplementary Figure S2 (Supporting Information)). The single residue (Gln85) that consistently fell in the disallowed region of the Ramachandran plot is positioned on a loop, which is underdetermined in the structure calculations due to relatively fewer NOE restraints observed for this segment of the protein. The conformational and energetic analyses on the ensemble of the 20 lowest energy structures performed by PROCHECK-NMR are reported in Table 1.

The overall three-dimensional fold of apo NosL consists of two structurally similar and relatively independent domains composed of a mixed α/β topology in which each domain contains a novel $\beta\beta\alpha\beta$ motif (Figure 4). The second and third β strands within each motif (β2 and β3 of sheet A and β6 and β7 of sheet B) are connected by an α-helix via a right-handed crossover, packing each helix against the face of the respective attached β sheet (Figure 4A). Extensive searches conducted to identify domains structurally related to apo NosL's $\beta\beta\alpha\beta$ motif using the programs FATCAT, SCOP, VAST, and DALI revealed no matches to this domain in the database (*49*, *52*−*54*). Backbone atoms of the three β strands and α-helix of each motif superpose with an rmsd of 1.81 Å (Figure 4B), despite the fact that the sequence identity of the aligned residues within the secondary structure elements is only 11% in *A. cycloclastes*. The close structural relationship between the two domains of apo NosL may be an indication that the present-day fold of the protein is the result of an ancient gene duplication event.

The two $\beta\beta\alpha\beta$ domains are connected by a short 3_{10} helix that forms a hinge between them and projects outward into solvent (Figure 5), in which the slowly exchanging amide proton of Ala97 is involved in formation of a hydrogen bond with the carbonyl oxygen of Ala94, both of which are highly conserved residues. The two domains are almost perpendicular to each other and rotated ∼80° apart, and arranged in a twisted butterfly-like configuration that creates a large solvent-accessible cleft between them which bisects the structural core of the protein (Figure 5). The α1 helix forms the interface between the two lobes, interacting with residues from the face of sheet A and with sheet B in an edge-on manner, partially burying the N-terminal end of the helix between the two sheets (Figure 5A−C). Due to the orientation of the two domains, the buried surface area of apo NosL is relatively small, which, in conjunction with the many loops, generates an irregular surface with many clefts available for potential ligand− and protein−protein interactions (Figures 5 and 6). All of the four loops in apo NosL are solvent-exposed, consistent with fast amide H/D exchange, except for several residues in the long loop encompassing residues Met76−Gly89 (loop β3/β4), in which several of the amide protons are protected from rapid H−D exchange with solvent (Figure 5).

Residues surrounding the wide cleft between the two β sheets create a positive patch of electrostatic surface potential due to the presence of residues Arg60, Arg53, and Arg106 (Figure 6). In contrast, the interior of the cavity is relatively neutral. The remainder of the protein surface displays a substantial negative potential, especially near the C-terminal end of the structure, which arises from the clustering of acidic residues Asp142, Asp139, Asp158, Glu150, Glu154, Glu160, and Asp159 (Figure 6). Residues on the C-terminal side of the short 3_{10} helix formed by Leu137, Ala138, and Asp139 form a small hydrophobic cluster, which includes the side chains of the conserved residues Ile140, Leu137, and Tyr99 (Figure 6). These contacts extend over the top of β sheet B in an irregular conformation and constitute the last ordered region of apo NosL.

Structural Homology to MerB. A search of the RCSB Protein Data Bank using the DALI server identified only one statistically significant structural homologue to the structure of apo NosL: MerB, an organomercury lyase (PDB code 1S6L, *Z*-score = 4.0) (*55*). The superposition of the two proteins generated by MOLMOL (*45*) is shown in Figure 7. Figure 7A displays the structural alignment of apo NosL and full-length MerB, whereas 7B depicts the structural superposition of the two proteins excluding the N-terminal

FIGURE 3: Ensemble of 20 low-energy apo NosL protein structures derived from the NMR data. The stereoview depicts the overlay of backbone heavy atoms (N, Ca, and C′) for residues 35−160 for 20 lowest-energy structures of apo NosL relative to the mean structure. Figure 3 was generated using the MOLMOL (*45*) software. The set of 20 structures displayed in the figure was selected for final analysis from an initial set of 100 calculated structures using the "Ambiguous Restraints for Iterative Assignment" algorithm of ARIA 1.2 (*40*).

Table 1: Experimental Restraints Used in the Structure Calculations of Apo NosL and Statistical Analysis of the 20 Lowest Energy Structures[a]

Experimental NMR Restraints Used for Structure Calculations	
ARIA NOEs	
H−CH	1589
H−NH	851
unambiguous	851
ambiguous	607
total	1458
Manual NOEs	
H−CH and H−NH	112
H-bond distance restraints	76
Structural Statistics for 20 Lowest Energy Water-Refined Apo-NosL Structures	
Root-Mean-Square Deviations Relative to Average Structure (Å)	
backbone (C^{α}, C′, N) atoms in 2nd structure	0.52 ± 0.14
backbone all residues	1.33 ± 0.44
heavy atoms in 2nd structure	0.88 ± 0.14
heavy atoms in all residues	1.70 ± 0.43
Restraint Violations	
NOE distances with violations >0.5 Å	0.2 ± 0.4
dihedral with violations >5°	0.6 ± 0.8
Final Energies from Simulated Annealing (kcal/mol)	
F_{vdw}	−393 ± 21
F_{ele}	−4338 ± 79
Deviation from Idealized Geometry	
bonds (Å)	0.0040 ± 0.0002
angles (deg)	0.55 ± 0.02
impropers (deg)	1.61 ± 0.14
Ramachandran Analysis (% of All Residues)	
residues in most favored regions	83.3
residues in additional allowed regions	13.7
residues in generously allowed regions	2.0
residues in disallowed regions	1.0

[a] Root-mean-squared deviations (rmsds) have been calculated for core regions of defined secondary structure and include residues belonging to β strands β1, β2, β3, β4, β5, β6, β7, and helices α1 and α2.

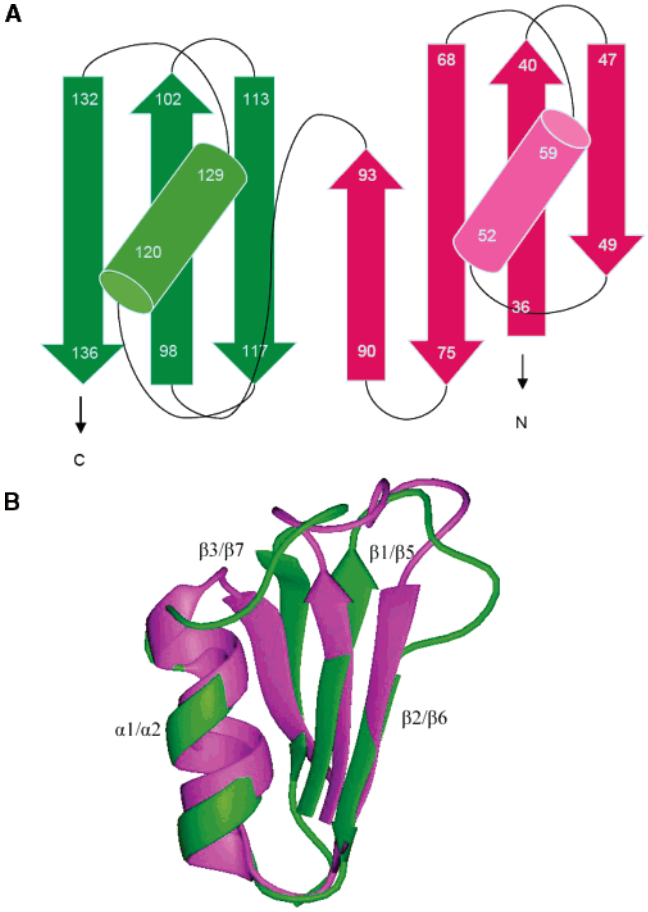

FIGURE 4: (A) Schematic diagram of the topological arrangement of secondary structural elements in apo NosL. The two structurally homologous domains of apo NosL are color-coded in green and magenta, respectively, and illustrate the right-handed crossover between the α-helix and β-sheet of each $\beta\beta\alpha\beta$ motif. (B) Structural alignment of the two $\beta\beta\alpha\beta$ domains of apo NosL. Domain 1 (composed of residues Ala36−Asp75) is displayed in magenta with strands β1, β2, β3 and helix α1 labeled while domain 2 (encompassing residues Phe98−Ala136) is colored in green with strands β5, β6, β7 and α2 labeled. Backbone atoms for residues located in the secondary structural elements of each domain align with a root-mean-square deviation (rmsd) of 1.81 Å, with the largest rmsd variations corresponding chiefly to residues positioned in the loop spanning strands β1 and β2 and the loop bridging strands β5 and β6. Figure 4B was generated using MOLMOL (*45*).

domain of MerB which is absent in the structure of apo NosL. Backbone rmsd for the aligned regions of the two proteins is 3.74 Å, demonstrating that, aside from differences described below, the core of the 3D structure of apo NosL derived from the NMR ensemble aligns well with the 3D structure of MerB, despite low sequence identity (<20%) between the two proteins. Consisting of three separate antiparallel β sheets and six α-helices, MerB is larger than apo NosL and possesses an N-terminal domain that is not present in apo NosL. MerB's N-terminal domain is composed of three α-helices and two short β strands combined to form a winged-helix $\alpha\alpha\alpha\beta\beta$ fold that is proposed to function in protein−protein interactions (*55*). Interestingly, this is the only region of MerB that exhibits structural similarity to other

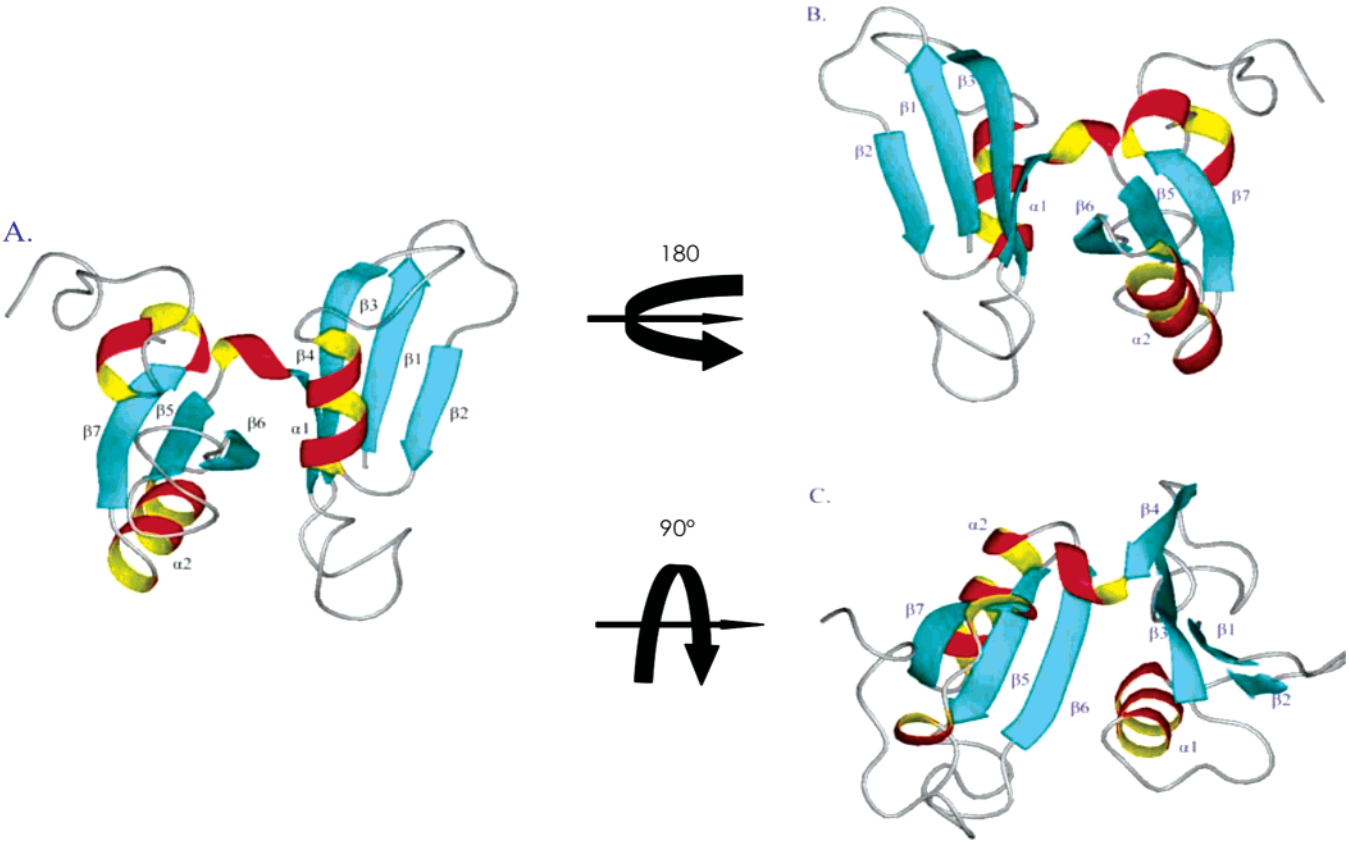

FIGURE 5: Ribbon diagrams of a representative low-energy conformer of apo NosL viewed from various orientations, and generated using the MOLMOL software (*45*). (A) The β sheets are depicted in cyan, helices in red and yellow. The protein's β strands β1, β2, β3, β4, β5, β6, and β7, and helices α1, and α2, as detailed in the text, are labeled. (B) A view of the apo NosL structure rotated by 180° relative to the orientation in panel A, in which the 3_{10} "hinge" is projecting toward the viewer. (C) The image has been rotated 90° relative to the orientation in panel A and illustrates the perpendicular relationship of the two β sheets.

proteins in the Protein Data Bank. Although the corresponding N-terminal region of apo NosL is not modeled in the present calculations, its smaller size and lack of secondary structure are not consistent with the presence of a winged-helix fold.

Apart from the N-terminal domain, a large portion of the MerB protein adopts a unique fold that it shares with apo NosL (*55*). The two β sheets of apo NosL, sheets A and B, superpose with the two C-terminal β sheets (sheets B and C) of MerB, with the exception of an extra strand (β7) in sheet B of MerB (Figure 8A−C). The unusual perpendicular orientation of the two sheets, including some of the molecular interactions between secondary structural elements, is common to the two proteins. The α1 helix of apo NosL aligns with the short α4 helix/coil of MerB but is ill-defined in MerB due to the sparse number of NMR-derived restraints for this region. Finally, in the place of the disordered C-terminus of apo NosL, MerB contains a long α-helix (α6) that is positioned between sheets B and C. Interestingly, the long flexible loop (β8/β9) of MerB containing the mercury binding residue Cys159 is spatially homologous to loop β5/β6 in the apo NosL structure (Figure 8), which contains one of two recognizable motifs conserved within the NosL family, G(G/A)XMGA, and may provide one of the few strictly conserved sulfur ligands.

DISCUSSION

Structural Homology of NosL and MerB. The unexpected structural similarity between apo NosL and the recently discovered fold of MerB, an organomercuric lyase that is responsible for broad mercury resistance in bacteria, provides unanticipated insight into the potential role NosL serves in the assembly of N_2OR. MerB binds a variety of organometallic-Hg(II) compounds, very toxic forms of mercury, and, with the aid of 2 equiv of a physiological thiol, cleaves the carbon bond via a rare S_E2 protonolysis mechanism, ultimately delivering Hg(II) to MerA for further detoxification (*55*, *56*). MerB and apo NosL are thus far the only members of a new structural superfamily, each containing two perpendicularly arranged $\beta\beta\alpha\beta$ motifs. In the MerB structure, the two motifs have acquired functional specialization, evidenced by the positioning of the two metal binding residues of each domain in distinct locations (*55*).

Apo NosL and MerB both exhibit a similar and unusual perpendicular arrangement of two β sheets, creating a strikingly large cleft between them. While the preservation of this cleft in both proteins suggests an important function for this surface structure, there are marked differences between apo NosL and MerB with respect to specific architecture and to the identity of residues lining the clefts. Very few residues are conserved between the two proteins, strongly suggesting that apo NosL does not bind DTT or monothiol cofactors that bind within the cleft structure of MerB and that are associated with enzymatic turnover (*56*). Nevertheless, the relative overabundance of hydrophobic and conserved residues lining the cleft of apo NosL (Figure 6) suggests that this region may take part in protein−protein interactions, although no specific association between

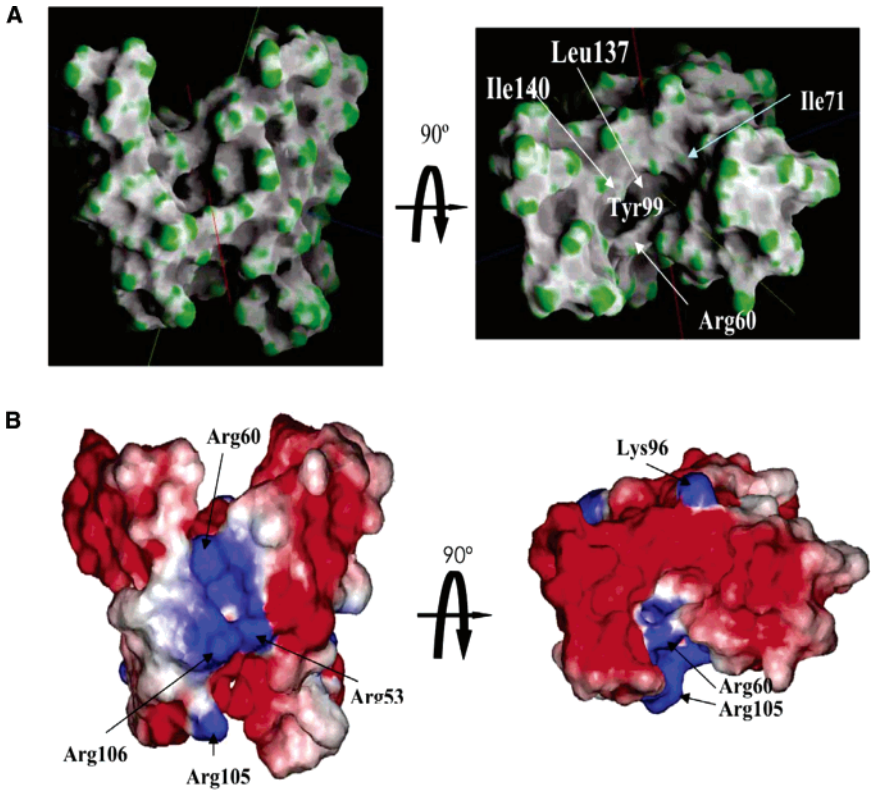

FIGURE 6: (A) Diagram of the molecular surface of apo NosL. The picture on the right-hand side depicts the large cleft between the two $\beta\beta\alpha\beta$ domains of the protein and the irregular surface created by multiple solvent-exposed loops. The picture on the left-hand side has been rotated by 90° and displays a view of the protein down a deep pocket created by the interactions of the protein structural elements α1, β1, β3, and β6, as described in the text. Figure 6A was generated with the GRASP (*47*) software and contoured according to surface curvature to emphasize depth. (B) Electrostatic surface potential of apo NosL displayed from two orientations of the protein, and generated using GRASP (*47*). The right-hand-side figure outlines the positively charged, basic patch surrounding the pocket created by residues Arg106, Arg53, and Arg60. The figure on the left-hand side is a view of apo NosL down its cleft structure.

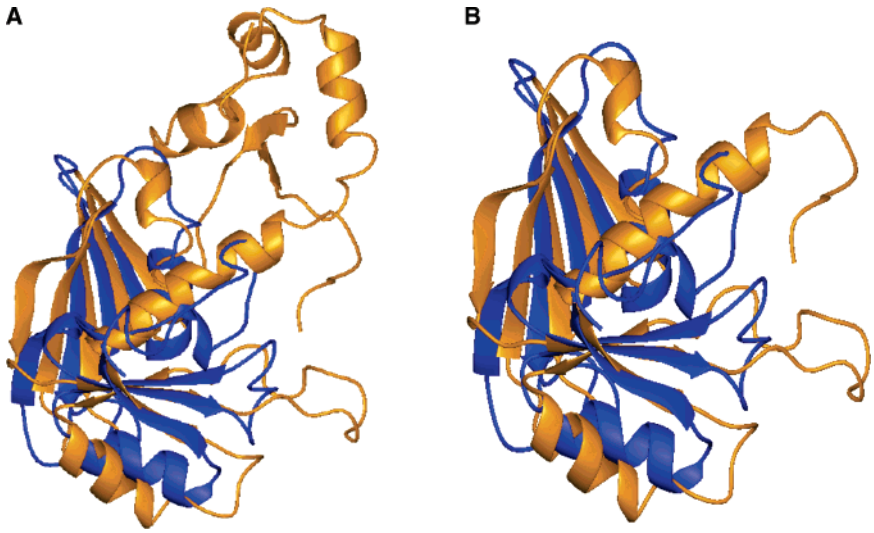

FIGURE 7: Structural comparison between MerB and apo NosL. (A) Superposition of structural elements of the full-length MerB protein with apo NosL. The secondary structural elements of both proteins are depicted as ribbon diagrams with MerB colored in brown and apo NosL in dark blue. The two antiparallel β sheets and helix α2 of apo NosL align closely with structural elements of MerB, while helix α1 overlays with a coil. MerB possesses a long helix (shown at a 45° angle) in place of the less well-defined C-terminus of apo NosL. (B) The structural alignment shown in this panel is similar to the one shown in panel A except that the N-terminal domain of MerB, absent in apo NosL, has been omitted for clarity.

NosL and other proteins or biomolecules has thus far been reported.

While the common fold is evidence for an ancestral link between NosL and MerB, there is no evidence that NosL functions as an organometallic lyase. NosL does not possess two conserved cysteine residues implicated in the organometallic bond cleavage reaction of MerB. Furthermore, the very low sequence homology to MerB falls below the limit at which functional conservation can be expected. Despite inherent limitations of inferring function from structural similarities, some conserved mechanistic feature that relies on the integrity of a common fold is often retained within a

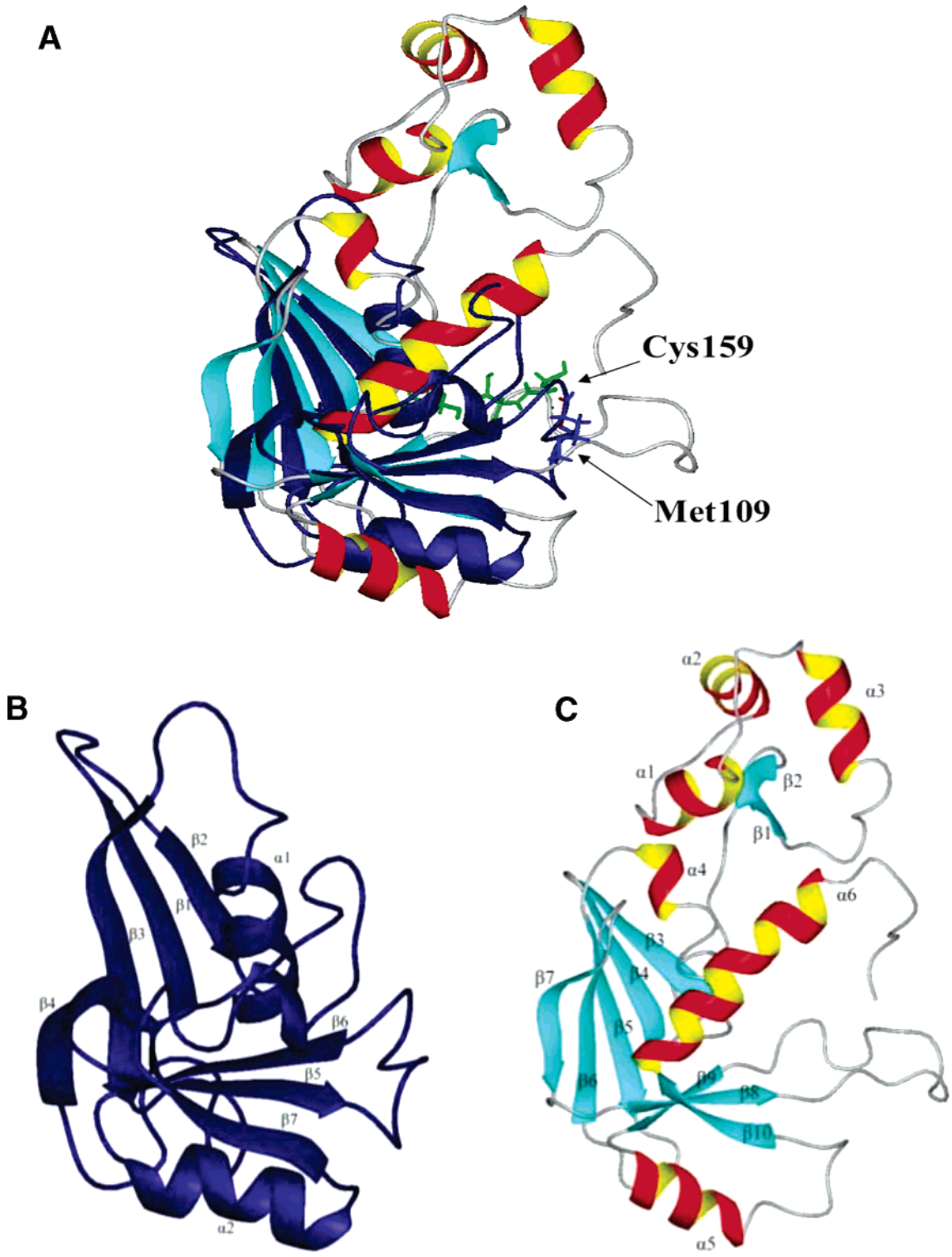

FIGURE 8: (A) Structural alignment of apo NosL with full-length MerB protein including depiction of metal-binding ligands. The β strands of MerB are displayed in cyan, while α helices are colored in yellow and red. The structural elements of apo NosL are shown in dark blue. One of the proposed copper ligands for NosL, Met109, is shown in dark blue and positioned on a loop spanning β strands 5 and 6, which aligns closely with one of the long loops (depicted in dark gray) of the MerB protein. The mercury binding ligands of MerB, Cys159 and Cys96, are colored in green. The individual structures of apo NosL and MerB (as reported in ref 55) are shown separately in panels B and C, respectively, to aid the reader in assessing similarities and differences between the two proteins. In this figure, the titled images of apo NosL and MerB have been gyrated away from the viewer to emphasize the unusual perpendicular orientation of the two antiparallel β sheets relative to each other in each protein.

protein superfamily (*57*). In the case of NosL and MerB, this conserved mechanistic feature would appear to require the presence of a large cleft between the two $\beta\beta\alpha\beta$ domains contiguous with a mononuclear metal binding site.

Copper(I) Ligands in NosL. Previous studies suggest that Cu(I) in NosL is coordinated by one nitrogen/oxygen and two sulfur ligands (*18*). Met109 (corresponding to Met127 in the numbering scheme of the NosL sequence deposited

in the PDB) is one of few conserved residues capable of providing a sulfur ligand for metal coordination, and resides within one of the two motifs that characterize the NosL family of sequences, G(G/A)XMGA. The high glycine content of this region of the protein suggests that flexibility may be an important feature of this motif. Consistent with a role in Cu(I) binding, this sequence motif is located on the $\beta5/\beta6$ loop of apo NosL which structurally superposes with the $\beta8/\beta9$ loop of MerB that contains the Hg(II)-binding residue Cys159 (Figure 8). In addition, the side chain of Met109 is solvent-exposed in the apo structure of NosL and is therefore available for interaction with a metal ion. Although the identity of the other copper ligands remain unknown at this time, there are no other sulfur ligands located within the same β sheet (sheet B) as Met109, indicating that the other metal ligands must be provided by a portion of the other $\beta\beta\alpha\beta$ domain of NosL, or by the N-terminal segment of the protein not modeled in our structures.

Met26 (i.e. Met44 in the PDB sequence) is highly conserved among NosL sequences and could serve as the second sulfur ligand identified in the EXAFS data (*18*). Met ligation of Cu(I) in NosL is consistent with the relatively recent discovery of a high-affinity methionine-rich copper binding motif, MX_nM, that is specific for metal uptake in the oxidizing environment of the periplasm (*19*−*21*). Unfortunately, because the N-terminus of apo NosL containing Met26 and the cysteine residue (Cys24) previously implicated in metal binding is disordered, the 3D structure of apo NosL provides no additional insight as to the possibility of Cys24 and Met26 of being sulfur ligands for Cu(I) chelation to the protein.

Role of NosL in N_2OR Assembly. Despite the difficulty of detecting common functional elements between apo NosL and its structural homologue MerB, it is highly likely that both proteins bind metal ions in a solvent-accessible state contiguous with a large binding cleft, implying that metal ion binding and subsequent release to a binding partner may be a common chemical or mechanistic characteristic of the two proteins. Given the common structural features in the two proteins, a role for NosL in copper or copper/sulfur transfer may be envisioned and is consistent with metallochaperone activity.

Most metallochaperones bind their metals via residues clustered within a relatively few sequential number of amino acids, unlike NosL in which the metal site architecture appears to involve discontinuous regions of the polypeptide. In this respect NosL is similar to the metallochaperone Sco1, a protein involved in assembly of the Cu_A dinuclear copper center of cytochrome *c* oxidase, and with proposed copper transfer activity in which the metal center is formed by residues from nonadjacent structural elements (*58*). Sco1 is also unique among known metallochaperones because it anchors to the membrane via interaction of an N-terminal transmembrane helix with membrane lipids (*59*). Protein anchoring to the membrane is reminiscent of NosL, where the mature protein is predicted to anchor to the outer cellular membrane via a thioether bond between a lipid and the protein's N-terminal cysteine (*8*, *11*, *15*, *16*, *18*).

Studies to determine the minimal set of proteins required for N_2OR biogenesis have shown that NosL is not strictly essential for either Cu_Z or Cu_A assembly in N_2OR (*5*). However, if NosL is only required under copper deficient conditions, as is the case with other metal chaperones, it is possible that sufficient copper depletion was not achieved in NosL knockout experiments, such that potential metal delivery function was not detected. It is also conceivable that a NosL paralogue exists that can replace its function in knockout strains, similar to the way NirX can substitute for NosX, a redox component of the *nos* cluster (*60*). If, in fact, NosL is shown to serve as a metallochaperone, it possesses a unique fold among this increasingly structurally diverse class of proteins.

ACKNOWLEDGMENT

We thank Dr. Robert Tyler for technical assistance with use of the ARIA software and apo NosL protein structure calculations, and Doreen Brown for critical reading of the manuscript. Several NMR spectra were acquired on a Varian 800 INOVA (800 MHz) instrument at the Environmental Molecular Sciences Laboratory (EMSL), sponsored by the Department of Energy's Office of the Biological and Environmental Research and located at the Pacific Northwest National Laboratory (PNNL) (Proposal 10299).

SUPPORTING INFORMATION AVAILABLE

List of NMR experiments and experimental parameters used for the NMR structure determination of apo NosL (Supplementary Table 1); multiple sequence alignment of seven NosL sequences from organisms with well-characterized N2OR sequences (Supplementary Figure S1); Ramachandran dihedral angle plot for 20 low energy NMR structures of apo NosL used in the final structural analysis (Supplementary Figure S2). This material is available free of charge via the Internet at http://pubs.acs.org.

REFERENCES

1. Farrar, J. A., Zumft, W. G., and Thomson, A. J. (1998) CuA and CuZ are variants of the electron transfer center in nitrous oxide reductase, *Proc. Natl. Acad. Sci. U.S.A. 95*, 9891−6.
2. Farrar, J. A., Neese, F., Lappalainen, P., Kroneck, P. M. H, Saraste, M., Zumft, W. G., and Thomson, A. J. (1996) The electronic structure of CuA: a novel mixed-valence dinuclear copper electron transfer center, *J. Am. Chem. Soc. 118*, 11501−14.
3. Rasmussen, T., Berks, B. C., Sanders-Loehr, J., Dooley, D. M., Zumft, W. G., and Thornson, J. A. (2000) The catalytic center in nitrous oxide reductase CuZ is a copper sulfide cluster, *Biochemistry 39*, 12753−6.
4. Fath, M. J., and Kolter, R. (1993) ABC transporters: bacterial exporters, *Microbiol. Rev. 57*, 995−1017.
5. Wunsch, P., Herb, M., Wieland, H., Schiek, U. M., and Zumft, W. G. (2003) Requirements for Cu(A) and Cu-S center assembly of nitrous oxide reductase deduced from complete periplasmic enzyme maturation in the nondenitrifier Pseudomonas putida, *J. Bacteriol. 185*, 887−96.
6. Honisch, U., and Zumft, W. G. (2003) Operon structure and regulation of the nos gene region of Pseudomonas stutzeri, encoding an ABC-Type ATPase for maturation of nitrous oxide reductase, *J. Bacteriol. 185*, 1895−902.
7. Ciccarelli, F. D., Copley, R. R., Doerks, T., Russell, R. B., and Bork, P. (2002) CASH—a beta-helix domain widespread among carbohydrate-binding proteins, *Trends Biochem. Sci. 27*, 59−62.
8. Dreusch, A., Riester, J., Kroneck, P. M. H., Zumft, W. G. (1996) Mutation of the conserved Cys165 outside of the CuA domains destabilizes nitrous oxide reductase but maintains its catalytic activity, *Eur. J. Biochem. 237*, 447−453.
9. Inatomi, K. (1998) Analysis of the nitrous oxide reduction genes, nosZDFYL, of Achromobacter cycloclastes, *DNA Res. 5*, 365−71.
10. Narita, S., Matsuyama, S., and Tokuda, H. (2004) Lipoprotein trafficking in Escherichia coli, *Arch. Microbiol. 182*, 1−6.

11. McGuirl, M. A., Nelson, L. K., Bollinger, J. A., Chan, Y. K., and Dooley, D. M. (1998) The nos (nitrous oxide reductase) gene cluster from the soil bacterium Achromobacter cycloclastes: cloning, sequence analysis, and expression, *J. Inorg. Biochem. 70*, 155−69.
12. Bedmar, E. J. (1998) Bradyrhizobium japonicum nosRZDFYLX gene cluster for nitrous oxide reduction, NCBI Web Page, Genbank Accession No. AJ002531, accessed August 2006.
13. Stover, C. K., Pham, X. Q., Erwin, A. L., Mizoguchi, S. D., Warrener, P., Hickey, M. J., Brinkman, F. S., Hufnagle, W. O., Kowalik, D. J., Lagrou, M., Garber, R. L., Goltry, L., Tolentino, E., Westbrock-Wadman, S., Yuan, Y., Brody, L. L., Coulter, S. N., Folger, K. R., Kas, A., Larbig, K., Lim, R., Smith, K., Spencer, D., Wong, G. K., Wu, Z., Paulsen, I. T., Reizer, J., Saier, M. H., Hancock, R. E., Lory, S., and Olson, M. V. (2000) Complete genome sequence of Pseudomonas aeruginosa PA01, an opportunistic pathogen, *Nature 406*, 959−64.
14. Hoeren, F. U., Berks, B. C., Ferguson, S. J., and McCarthy, J. E. (1993) Sequence and expression of the gene encoding the respiratory nitrous oxide reductase from Paracoccus denitrificans: new and conserved structural and regulatory motifs, *Eur. J. Biochem. 218*, 49−50.
15. Zumft, W. G., Viebrock-Sambale, A., and Braun, C. (1990) Nitrous oxide reductase from denitrifying Pseudomonas stutzeri. Genes for copper-processing and properties of the deduced products, including a new member of the family of ATP/GTP-binding proteins, *Eur. J. Biochem. 192*, 591−9.
16. Chan, Y. K., McCormick, W. A., and Watson, R. J. (1997) A new nos gene downstream from nosDFY is essential for dissimilatory reduction of nitrous oxide by Rhizobium (Sinorhizobium) meliloti, *Microbiology 143* (Part 8), 2817−24.
17. Sabaty, M., Schwintner, C., Cahors, S., Richaud, P., and Vermeglio, A. (1999) Nitrite and nitrous oxide reductase regulation by nitrogen oxides in Rhodobacter sphaeroides f. sp. denitrificans IL106, *J. Bacteriol. 181*, 6028−32.
18. McGuirl, M. A., Bollinger, J. A., Cosper, N., Scott, R. A., and Dooley, D. M. (2001) Expression, purification, and characterization of NosL, a novel Cu(I) protein of the nitrous oxide reductase (nos) gene cluster, *J. Biol. Inorg. Chem. 6*, 189−95.
19. Arnesano, F., Banci, L., Bertini, I., and Thompsett, A. R. (2002) Solution structure of CopC: a cupredoxin-like protein involved in copper homeostasis, *Structure 10*, 1337−47.
20. Loftin, I. R., Franke, S., Roberts, S. A., Weichsel, A., Heroux, A., Montfort, W. R., Rensing, C., and McEvoy, M. M. (2005) A novel copper-binding fold for the periplasmic copper resistance protein CusF, *Biochemistry 44*, 10533−40.
21. Wernimont, A. K., Huffman, D. L., Finney, L. A., Demeler, B., O'Halloran, T. V., and Rosenzweig, A. C. (2003) Crystal structure and dimerization equilibria of PcoC, a methionine-rich copper resistance protein from Escherichia coli, *J. Biol. Inorg. Chem. 8*, 185−94.
22. O'Halloran, T. V., and Culotta, V. C. (2000) Metallochaperones, an intracellular shuttle service for metal ions, *J. Biol. Chem. 275*, 25057−60.
23. Marion, D., Ikura, M., Tschudin, R., and Bax, A. (1989) Rapid Recording of 2D Nmr-Spectra Without Phase Cycling−Application to the Study of Hydrogen-Exchange in Proteins, *J. Magn. Res. 85*, 393−9.
24. Delaglio, F., Grzesiek, S., Vuister, G. W., Zhu, G., Pfeifer, J., and Bax, A. (1995) NMRPipe: a multidimensional spectral processing system based on UNIX pipes, *J. Biomol, NMR 6*, 277−93.
25. Garrett, D. S., Powers, R., Gronenborn, A. M., and Clore, G. M. (1991) A common sense approach to peack picking in two-, three-, and four-dimensional spectra using automatic computer analysis of contour diagrams, *J. Magn. Reson. 95*, 214−20.
26. Johnson, B. A. (2004) Using NMRView to visualize and analyze the NMR spectra of macromolecules, *Methods Mol. Biol. 278*, 313−52.
27. Bodenhausen, G., and Ruben, D. J. (1980) Natural Abundance Nitrogen-15 NMR by Enhanced Heteronuclear Spectroscopy, *Chem. Phys. Lett. 69*, 185−9.
28. Shaka, A. J. K., J., Freeman, R. (1983) Evaluation of a new broadband decoupling sequence: WALTZ-16, *J. Magn. Reson. 53*, 313−40.
29. Kay, L. E., Ikura, M., Tschudin, R., and Bax, A. (1990) Three-dimensional triple-resonance NMR spectroscopy of isotopically enriched proteins, *J. Magn. Reson. 89*, 496−514.
30. Wittekind, M., and Mueller, L. (1993) HNCACB, a high-sensitivity 3D NMR experiment to correlate amide-proton and nitrogen resonances with {alpha} and proton and nitrogen resonances with alpha and beta carbon resonances in proteins, *J. Magn. Reson. 101*, 201−5.
31. Grzesiek, S., and Bax, A. (1992) Correlating backbone amide and side chain resonances in larger proteins by multiple relayed triple resonance NMR, *J. Am. Chem. Soc. 114*, 6291−3.
32. Grzesiek, S., Anglister, J., and Bax, A. (1993) Correlation of backbone amide and aliphatic side-chain resonances in 13C/15N enriched proteins by isotropic mixing of 13C magnetization, *J. Magn. Reson. 101*, 114−9.
33. Vuister, G. W., and Bax, A. (1992) Resolution enhancement and spectral editing of 13C-enriched proteins by homonuclear broadband 13C decoupling, *J. Magn. Reson. 98*, 428−35.
34. Bax, A., Clore, M., and Gronenborn, A. M. (1990) 1H-1H correlation via isotropic mixing of 13C magnetization, a new three-dimensional approach for assigning 1H and 13C spectra of 13C-enriched proteins, *J. Magn. Reson. 88*, 425−31.
35. Shaka, A. J., Lee, C. J., and Pines, A. (1988) Iterative schemes for bilinear operators; application to spin decoupling, *J. Magn. Res. 77*, 274−93.
36. Kay, L. E., Marion, D., and Bax, A. (1989) Practical Aspects of 3D Heteronuclear NMR of Proteins, *J. Magn. Reson. 84*, 72−84.
37. Marion, D., Kay, L. E., Sparks, S. W., Torchia, D. A., and Bax, A. (1989) Three-dimensional heteronuclear NMR of 15N-labeled proteins, *J. Am. Chem. Soc. 111*, 1515−7.
38. Bax, A., Clore, G. M., Driscoll, P. C., Gronenborn, A. M., Ikura, M., and Kay, LE. (1990) Practical Aspects of Proton-Carbon-Carbon-Proton Three-Dimensional Correlation Spectroscopy of 13C-Labeled Proteins, *J. Magn. Reson. 87*, 620−7.
39. Nilges, M., Macias, M. J., O'Donoghue, S. I., and Oschkinat, H. (1997) Automated NOESY interpretation with ambiguous distance restraints: the refined NMR solution structure of the pleckstrin homology domain from beta-spectrin, *J. Mol. Biol. 269*, 408−22.
40. Linge, J. P., O'Donoghue, S. I., and Nilges, M. (2001) Automated assignment of ambiguous nuclear overhauser effects with ARIA, *Methods Enzymol. 339*, 71−90.
41. Linge, J. P., Habeck, M., Rieping, W., and Nilges, M. (2003) ARIA: automated NOE assignment and NMR structure calculation, *Bioinformatics 19*, 315−6.
42. Linge, J. P., Williams, M. A., Spronk, C. A., Bonvin, A. M., and Nilges, M. (2003) Refinement of protein structures in explicit solvent, *Proteins 50*, 496−506.
43. Brunger, A. T., Adams, P. D., Clore, G. M., DeLano, W. L., Gros, P., Grosse-Kunstleve, R. W., Jiang, J. S., Kuszewski, J., Nilges, M., Pannu, N. S., Read, R. J., Rice, L. M., Simonson, T., and Warren, G. L. (1998) Crystallography & NMR system: A new software suite for macromolecular structure determination, *Acta Crystallogr., D: Biol. Crystallogr. 54* (Part 5), 905−21.
44. Cornilescu, G., Delaglio, F., and Bax, A. (1999) Protein backbone angle restraints from searching a database for chemical shift and sequence homology, *J. Biomol. NMR 13*, 289−302.
45. Koradi, R., Billeter, M., and Wuthrich, K. (1996) MOLMOL: a program for display and analysis of macromolecular structures, *J. Mol. Graphics 14*, 29−32, 51−5.
46. Laskowski, R. A., Rullmannn, J. A., MacArthur, M. W., Kaptein, R., and Thornton, J. M. (1996) AQUA and PROCHECK-NMR: programs for checking the quality of protein structures solved by NMR, *J. Biomol. NMR 8*, 477−86.
47. Nayal, M., Hitz, B. C., and Honig, B. (1999) GRASP: a server for the graphical representation and analysis of structures, *Protein Sci. 8*, 676−9.
48. Holm, L., and Sander, C. (1996) Alignment of three-dimensional protein structures: network server for database searching, *Methods Enzymol. 266*, 653−62.
49. Holm, L., and Sander, C. (1996) Mapping the protein universe, *Science 273*, 595−603.
50. Taubner, L. M., McGuirl, M. A., Dooley, D. M., and Copie, V. (2004) 1H, 13C, 15N backbone and side chain resonance assignments of apo NosL, a novel copper(I) binding protein from the nitrous oxide reductase gene cluster of Achromobacter cycloclastes, *J. Biomol. NMR 29*, 211−2.
51. Wishart, D. S., Bigam, C. G., Holm, A., Hodges, R. S., and Sykes, B. D. (1995) 1H, 13C and 15N random coil NMR chemical shifts of the common amino acids. I. Investigations of nearest-neighbor effects, *J. Biomol. NMR 5*, 67−81.

52. Murzin, A. G., Brenner, S. E., Hubbard, T., and Chothia, C. (1995) SCOP: a structural classification of proteins database for the investigation of sequences and structures, *J. Mol. Biol. 247*, 536−40.
53. Ye, Y., and Godzik, A. (2004) FATCAT: a web server for flexible structure comparison and structure similarity searching, *Nucleic Acids Res. 32*, W582−5.
54. Madej, T., Gibrat, J. F., and Bryant, S. H. (1995) Threading a database of protein cores, *Proteins 23*, 356−69.
55. Di Lello, P., Benison, G. C., Valafar, H., Pitts, K. E., Summers, A. O., Legault, P., and Omichinski, J. G. (2004) NMR structural studies reveal a novel protein fold for MerB, the organomercurial lyase involved in the bacterial mercury resistance system, *Biochemistry 43*, 8322−32.
56. Benison, G. C., Di Lello, P., Shokes, J. E., Cosper, N. J., Scott, R. A., Legault, P., and Omichinski, J. G. (2004) A stable mercury-containing complex of the organomercurial lyase MerB: catalysis, product release, and direct transfer to MerA, *Biochemistry 43*, 8333−45.
57. Todd, A. E., Orengo, C. A., and Thornton, J. M. (2001) Evolution of function in protein superfamilies, from a structural perspective, *J. Mol. Biol. 307*, 1113−43.
58. Nittis, T., George, G. N., and Winge, D. R. (2001) Yeast Sco1, a protein essential for cytochrome *c* oxidase function is a Cu(I)-binding protein, *J. Biol. Chem. 276*, 42520−6.
59. Buchwald, P., Krummeck, G., and Rodel, G. (1991) Immunological identification of yeast SCO1 protein as a component of the inner mitochondrial membrane, *Mol. Gen. Genet. 229*, 413−20.
60. Saunders, N. F., Hornberg, J. J., Reijnders, W. N., Westerhoff, H. V., de Vries, S., and van Spanning, R. J. (2000) The NosX and NirX proteins of Paracoccus denitrificans are functional homologues: their role in maturation of nitrous oxide reductase, *J. Bacteriol. 182*, 5211−7.

BI061089+